EUROPEAN FUSION DEVELOPMENT AGREEMENT

EFDA–JET–PR(04)46

Yu.F. Baranov, C. Bourdelle, T. Bolzonella, M.De Baar, C.D. Challis, C.Giroud, N.C. Hawkes, E.Joffrin, V. Pericoli Ridolfini and JET EFDA contributors

Effect of Hysteresis in JET ITB Plasma with LHCD

Effect of Hysteresis in JET ITB Plasma with LHCD

Yu.F. Baranov[1], C. Bourdelle[2], T. Bolzonella[3], M.De Baar[4], C.D. Challis[1], C.Giroud[1], N.C. Hawkes[1], E.Joffrin[2], V. Pericoli Ridolfini[3] and JET EFDA contributors*

[1]EURATOM/UKAEA Fusion Association, Culham Science Centre, Abingdon Oxon OX14 3DB, UK
[2]Association EURATOM-CEA, CE de Cadarache, F-13108, S[t] Paul lez Durance, France.
[3]Associazione EURATOM-ENEA sulla Fusione, C.R. Frascati, Frascati , Italy.
[4]FOM instituut voor plasmafysica Rijnhuizen P.O. Box 1207, 3430 BE Nieuwegein, The Netherlands.
** See annex of J. Pamela et al, "Overview of Recent JET Results and Future Perspectives", Fusion Energy 2002 (Proc. 19[th] IAEA Fusion Energy Conference, Lyon (2002).*

Preprint of Paper to be submitted for publication in
Plasma Physics and Controlled Fusion

ABSTRACT

A strong ITB was sustained in a reversed shear discharge in JET during a long time interval after a significant reduction in plasma heating power. The observed ITB evolution is reminiscent of the effect of hysteresis. The mechanism of ITB sustainment was analysed. Modelling of the plasma heating and current profile were done using the TRANSP and JETTO transport codes. The resulting q-profile evolution was verified by comparison with the pitch angle $\delta = B_p/B_t$ deduced from Motional Stark Effect (MSE) measurements (where B_p and B_t are poloidal and toroidal magnetic field, respectively). Turbulence stability was analysed using the gyro-kinetic code Kinezero. It was shown that strong negative magnetic shear produced by LHCD and sustained mainly by the bootstrap current in the plasma core is responsible for the turbulence stabilisation. Stabilisation due to shear of the plasma rotation and finite β-stabilisation play a complimentary role. The effect of bootstrap and LH driven currents on magnetic shear in JET discharges was analysed.

1. INTRODUCTION

The transition to a state of improved confinement has been observed in many tokamaks. Such transition is associated with the formation of edge or internal transport barriers [1-4]. A reduction of heat transport inside the barriers occurs due to the suppression of the micro turbulence [2,3,5]. Transitions of several types have been discussed in literature [6]. In the first-order transition theory the radial electric field E_r is dominated by the poloidal plasma rotation term $E_r = -u_\theta B_{tor}$, where the velocity u_θ is proportional to the ion temperature gradient [7]. The radial shear in u_θ is proportional to $\partial^2 T_i/\partial r^2$, which directly relates to the E×B flow shear. Suppression of the turbulence occurs when the E×B flow shear exceeds the linear growth rate of the fluctuations [5]. The transition occurs, when the heat flux reaches some critical value Q_{crit}. It is accompanied by a discontinuous increase in the temperature gradient. Suppression of the turbulence causes a local reduction in the thermal conductivity providing a barrier for heat transport. Once established the barrier can be sustained at a heat flux level below Q_{crit}. This effect of hysteresis is an essential feature of barrier dynamics. The first order transition theory proposed initially for a description of the edge barrier was modified later for ITBs [8]. The second order transition theory describes the turbulence suppression due to the E×B flow shear produced by the Reynolds stress [9]. It is relevant to short time scale events of the order of several correlation times in contrast to the first order transition, which occurrs on the time scale of the pressure profile evolution. Heat transport induced by turbulence is proportional to the energy of the fluctuations in the aforementioned theories. The effect of the cross phase between the density and velocity fluctuations was discussed in [6] (see also the relevant references therein). It was recently found in a numerical simulation that the cross phase reduces the electron heat transport in configurations with strongly reversed magnetic shear, in accordance with experimental observation [10].

It was found in JET that a core ITB is formed in discharges with a current hole [11-15]. The ITB is located in a region of negative magnetic shear. It was demonstrated in the experiment described

below that ITBs formed at a sufficiently high level of the plasma heating power can be sustained for a long time after a significant reduction of the power. This is similar to the effect of hysteresis in barrier dynamics. The aim of this work is to investigate the mechanism of ITB sustainment in a discharge with negative magnetic shear after the heating power is stepped down. Special attention is paid to the relative roles of the turbulence stabilisation by magnetic shear, shear of the plasma rotation and finite β-stabilisation.

Results of modelling of the plasma heating and current drive in a pulse with an ITB in a current hole configuration is presented in the first section of this paper. The modelling was done using the TRANSP [16], JETTO [17] and LHCD [18] codes. The q profile was reconstructed using MSE measurements [19]. Conditions for ITB sustainement were analysed using the gyro-kinetic code Kinezero [20]. This code allows the determination of the linear growth rate γ_{lin} for the Ion Temperature Gradient and Trapped Electron mode (ITG/TEM) and Electron Temperature Gradient (ETG) modes in the framework of the gyro-kinetic model. The turbulence linear growth rates, predicted by Kinezero code, were compared with plasma rotation shearing rate $\omega_{E\times B}$ deduced from the JETTO code modelling. The results of the turbulence stability analysis are presented in the second section, which is followed by conclusions.

2. THE ROLE OF NON-INDUCTIVE CURRENT IN THE SUSTAINMENT OF SHEAR REVERSAL

The formation of a magnetic configuration with a hollow current profile by application of non-inductive current in the current ramp-up phase has routinely been used in a number of tokamaks [4,11,19,21]. The evolution of the main plasma parameters typical of a such scenario is shown in Figure 1 for JET Pulse No: 58178. Real time feedback control of the T_i gradient with neutral beam power was used in this pulse [22]. In the context of our investigation the time evolution of the ITB can be divided into three intervals. The first interval t<4.1s includes LHCD in the current ramp-up phase. The second interval 4.1s<t<7s corresponds to the main heating phase with combined (NBI and ICRH) power varying between 15MW and 20MW. This level of power exceeds the level required for the ion heat transport barrier formation in JET [11] for a current of I_p = 1.8MA and magnetic field B = 3T. The third time interval 7s<t<13s corresponds to a phase, when the plasma heating power is rapidly reduced from 15MW to 7MW and sustained at this low level.

According to criterion [23] used to identify ITBs in JET the electron heat transport barrier is formed, when parameter $\rho_e^* = -\sqrt{2m_pT_e/e}\,(dT_e/dR) / (B_\varphi T_e)$ exceeds the threshold value of 0.014. A contour plot of parameter ρ_e^* is shown in Figure 2. The electron heat transport barrier was formed very soon after the start-up of the LHCD preheat and continues until the end of the plasma heating phase. The ITB formation in this pulse was associated with negative magnetic shear [24] due to the application of LHCD in the current ramp-up phase [11,19]. The particle and ion heat transport barriers were formed after the start of the NBI and ICRF heating at t = 4.4s and survived until t = 13s, when the plasma additional heating was stopped. Electron, ion and density transport barriers were coincident

in space. We will focus our investigation of the ITB in the current flat-top phase beginning with the heating power step down at t = 8s and continuing until the end of the heating at t = 13s.

The current (q-profile) evolution was modelled using the TRANSP [16] code. The measured parameters such as plasma temperature, density and Z-effective were used in the TRANSP modelling. The LH driven current was simulated with the LHCD code, which is a combination of ray-tracing and 2-D Fokker plank code [18]. The results of the modelling were verified by comparing the ratio of the poloidal magnetic field B_p to the toroidal magnetic field B_θ deduced from MSE measurements [19] with those determined from the TRANSP calculations [25]. Figure 3 shows a comparison of the measured and calculated B_p/B_t. A region roughly between R=3m and 3.35m corresponds to an absolute value of $|B_p/B_t| < 0.02$. The total plasma current is small inside this region and it is associated with a current hole. The current hole 'boundary' corresponds to a location where $|B_p/B_t|$ starts to increase with radius. In this particular case the boundary is located between R = 3.3m and 3.4m on the low field side for the time range t = 5.35-6.35s (there are no MSE measurements in later phase). Formation and sustainment of shear reversal is connected directly with the non–inductive current j_{ext} produced in the plasma and induced Ohmic counter current. Figure 4 shows an evolution of different current components as deduced from TRANSP and LHCD modelling. The non-inductive components make up about 40%-45% of total current in the power step down phase. The bootstrap current I_{BS} is the main contributor to the non-inductive current until $t \approx 12$s, when LH driven current I_{lh} becomes greater than I_{bs}.

The formation of configurations with strongly reversed magnetic shear in the current ramp-up phase in JET has been discussed in detail in [19]. We concentrate here on the current flat top phase. Figure 5 shows profiles of the plasma temperature, current, q and magnetic shear after the power step down. The bootstrap current calculated using the NCLASS module [26] implemented in the TRANSP code is the dominant component of the current density in the plasma core ($r/a<0.3$). It is aligned with an ITB and produces a strong shear reversal. LH driven current in this relatively high density and high temperature phase is mainly peripheral and plays a complimentary role in the q-profile evolution, as will be discussed later. The ITB footpoint is close to the zero magnetic shear region (the footpoint is located in a region, where $|\nabla T|$ or $|\nabla n|$ varies abruptly from a large value inside the transport barrier to a small value outside the barrier).

The evolution of the measured electron temperature and calculated q-profile is shown in Figure 6 for the time interval following the heating power step down ($t>7$s). The magnetic shear reversal is sustained until the end of combined NBI and ICRH heating (t = 13s). As the bootstrap current is gradually reduced in the time interval t = 8-13s (see Figure 4) the negative magnetic shear region slowly shrinks towards the magnetic axis. The radius of the ITB footpoint follows roughly the location of a zero magnetic shear region. In spite of the reduction in the total bootstrap current it remains the largest component in the plasma core. The magnetic shear remains negative inside the ITB. The maximum temperature gradient is located in the region of large negative magnetic shear.

It has been already mentioned that LH driven current produced the shear reversal in the plasma

core during the current ramp-up phase, whereas it is mainly peripheral in the main heating phase. To demonstrate the effect of LHCD on the q-profile the current evolution was modelled for two hypothetical cases. Firstly, it was assumed that there was no LHCD in case 'h1'. Secondly, LH power was applied only in the current ramp up phase ($1.5s \leq t \leq 4s$) in the case 'h2'. Figure 7 shows current and q–profiles for these two hypothetical cases compared with the experimental case 'ex', where LHCD was applied during preheat and main heating phase ($1.5s \leq t \leq 13s$). In all cases the measured plasma parameters for Pulse No: 58178 were used in the modelling.

The modelling shows that LH driven current produces strong shear reversal in the plasma core ($r/a<0.3$) by the end of the current ramp-up phase ($t = 4s$) in cases 'ex' and 'h2' with central $q>15$ [19]. Only a moderate shear reversal is observed in case 'h1' (LHCD off) with central $q<4$. The large bootstrap current created after a start of the main heating ($t>4s$) replaces the LH driven current in the core in cases 'ex' and 'h2'. LH driven current becomes peripheral in case 'ex' for $t>4s$ as the temperature and density increase.

Much stronger shear reversal was obtained in the case 'ex' than in case 'h1' at $t=7.9s$, just before the high power step down (Figure 7(a)). A positive bootstrap current j_{bs}, NB driven current j_{nb} and induced negative Ohmic current j_{oh} are the main components of the total plasma current j_{tot} in the plasma core ($r/a \leq 0.4$). Note that the amplitude of j_{bs} and j_{oh} are larger in the 'ex' case (LHCD-on for $1.5s \leq t \leq 13s$) than in the 'h1' case (LHCD-off) for the same temperature and density. This result can be explained by a specific dependence of the bootstrap current on the poloidal magnetic field or safety factor: $j_{bs} \propto (1/Bq)\, \nabla P \propto q\, \nabla P$. For the same pressure gradient, larger j_{bs} is produced in the main heating phase in a configuration with large core q in case 'ex' than in case 'h1' with a smaller q in the core due to dependence of j_{bs} on q. Such dependence creates an effect of 'memory'. The q profile in the late phase depends on the q in the early phase (the mechanism discussed here is different from Faraday's law, which sustains the current on the skin time scale). This effect is demonstrated in Figure 7(b), where case 'ex' (LHCD-on for $1.5s \leq t \leq 13s$) is compared with the case 'h2' (LHCD-on for $1.5s \leq t \leq 4s$). An evolution of the q-profile is identical for these two cases during the current ramp up phase ($1.5s \leq t \leq 4s$) as the LH power is the same in both cases. The bootstrap current produced in the main heating phase before the power step down is very similar in both cases and there is only a small difference in q profile by $t = 7.9s$ as shown in Figure 7(b). In the absence of the bootstrap current the q profile relaxes in accordance with Faraday's law to a profile with weak shear reversal as shown in the same picture. The effect of 'memory' becomes weaker with time as can be seen from Figure 7(c) showing the current and q-profiles for cases 'ex' (LHCD-on for $1.5s \leq t \leq 13s$) and 'h2' (LHCD-on for $1.5s \leq t \leq 4s$) at $t = 13s$. Stronger shear reversal was found in case 'ex' with LHCD-on than in the 'h2' case with LHCD-off after the current ramp-up phase. It should also be noted that the zero magnetic shear region is shifted outward in case 'ex' with respect to the 'h2' case. The difference is more pronounced in the plasma core than in the periphery despite the peripheral location of the peak in j_{lh}. It is worth mentioning that LH current modifies the magnetic shear locally at the maximum of j_{lh}, which is located at $r/a \approx 0.6$ by $t = 13s$.

The modification is moderate with the magnetic shear reduced to $s \approx 0.63$ at the level of LH power of 2-2.5MW used in the experiment. Twice as much of LH power is required to reduce the shear to $s = -0.2$.

The modelling of the non-inductive current and the q-profile evolution for the Pulse No:58178 showed that the current hole and ITB are linked via the bootstrap current in the main heating phase(see Figures 3-7). The rate of the radial shift of the ITB after the heating power reduction predetermined the move of the negative magnetic shear region. The ITB or the pressure gradient evolution may depend on magnetic shear and the plasma flow shear. To clarify the relative role of this factors, the ITB evolution after the heating power step down has been modelled with the JETTO code using the transport model described and verified in [17]. In this model, the electron, ion and particle diffusivities were defined as a combination of the Bohm χ_B, gyro-Bohm χ_{gB}, and ion-neoclassical χ_i^{neo} diffusivities as follows:

$$\chi_e = 0.1\chi_{gB} + 10\,\chi_B, \qquad \chi_i = 0.1\chi_{gB} + 10\,\chi_B + 1.5\,\chi_i^{neo},$$

$$D_p = (1 + 0.3\rho)\,(\chi_e - \chi_i^{neo})\,(\chi_i - \chi_i^{neo})/(\chi_e - \chi_e^{neo} + \chi_i - \chi_i^{neo}) + D^{neo},$$

where, $\chi_{gB} = 5.10^{-6}\sqrt{T_e}|\nabla T_e|/B_\varphi^2$, $\chi_B = \chi_{B0}\Theta(\alpha_1 + \alpha_2 s + \alpha_3\,(\omega_{E\times B}/\gamma_{lin}))$,

with , $\chi_{B0} = 4\times10^{-5}\,Rq^2\,(T_e(0.8\rho_{max})/T_e(\rho_{max}) - 1)/|\nabla(n_eT_e)|/\,(n_eB_\varphi)$, ρ = r/a. SI units were are in expressions given above. The neoclassical heat χ_i^{neo} and particle D_i^{neo} diffusivities were deduced from the NCLASS modelling [26]. The linear growth rate was calculated in accordance with the Weiland model [27]. Both, NCLASS and Weiland model are implemented into JETTO code. The heating and particle sources used in the JETTO modelling were deduced from the TRANSP calculations, discussed above. The step function $\Theta(x) = 0$ for $x < 0$ and 1 for $x \geq 0$depends on the parameter $\tau = \alpha_1 + \alpha_2 s + \alpha_3(\omega_{E\times B}/\lambda_{lin})$, which allows to model a reduction of the anomalous diffusion χ_{B0} due to the effect of the magnetic shear and shear of the plasma rotation. Figure 8 shows a comparison of the plasma temperature, density and q-profiles deduced from measurements and from the JETTO predictive model described above. This result was obtained assuming that the argument τ of the step function Θ depends on the magnetic shear and dependence on the shearing rate is weak, i.e. $\alpha_1 = 0$, $\alpha_2 = 1$ and $\alpha_3 = 0.1$. Only the late phase of the discharge ($t > 6.5$s) was modelled in the case shown in Figure 8. The initial conditions at $t = 6.5$s were taken from the TRANSP modelling. The bootstrap current was varying from 0.53MA at $t = 9$s to 0.21MA at $t = 13$s, which is close to the result of the TRANSP modelling based on the measured plasma parameters (see Figure 4). The ITB footpoint and zero magnetic shear gradually move to the magnetic axis with a rate similar to the rate observed in the experiment. The effect of the flow shear stabilisation on the radial movement of the ITB is shown in Figure 9. Profiles of the plasma parameters were predicted using the JETTO predictive model for different values of $\alpha_3 = 0$, 0.1, 0.3. The direction of

the ITB footstep movement changes from inward for $\alpha_3 = 0$, and 0.1 to outward for $\alpha_3 = 0.3$. The ITB footstep is aligned radially exactly with $s = 0$ point in the case of $\alpha_3 = 0$, because the anomalous transport (Bohm) is reduced to zero in the region of $s<0$ in a framework of the model. A misalignment occurs and increases as a contribution of the term $\omega_{E\times B}/\gamma_{lin}$ $\omega_{E\times B}/\gamma_{lin}$ into τ increases with α_3 and anomalous transport is suppressed in the region of a positive s. A relation between shear flow and linear growth rate of the turbulence will be discussed in more details in the next section.

The conclusion that strong shear reversal, once created by LHCD, can be sustained for some time by only the bootstrap current in the plasma core is supported by the experimental data. In particular, very strong shear reversal associated with the 'current hole' in the plasma core, was observed in a Pulse No: 58383 throughout the high power heating phase ($4s<t<9s$). LH power was applied in this pulse only in the current ramp up phase in the time interval between 1.5s and 4s. The core ITBs are very similar in Pulse No's: 58178 and 58383 in both the LHCD and main heating phases (note that LH was applied all the time in Pulse No: 58178). However, we should stress the fact that the reversed shear region shrinks with time and the q-profile becomes monotonic in the presence of the bootstrap current alone. Larger off-axis non-inductive current outside ITB is required to sustain the negative magnetic shear in the plasma core in a steady state regime as it follows from the experiment and the modelling.

3. HEAT TRANSPORT AND TURBULENCE STABILITY ANALYSIS

The effect of hysteresis manifests itself in ITB sustainment after a significant reduction of the heating power in comparison with the power level, which is necessary to establish the ITB. As we mentioned in the introduction, the heat flux Γ through the barrier is the parameter relevant for the E×B flow shear, which may cause the turbulence suppression and produce the ITB [6]. It should be noted that a direct relationship exists between the heat flux and the E×B flow shear [6] in the case when the radial electric field is determined by the neoclassical poloidal plasma rotation. In JET, however, the main contribution to $E_r = (1/Z_i e n_i)\partial P_i/\partial r - u_\theta B_\varphi + u_\varphi B_\theta$ comes from the toroidal rotation $E_r = u_\theta B_\varphi$, which is determined by externally applied torque [28]. Here Z_i, n_i and P_i are the ion charge, density and pressure and $u_{\varphi,\theta}$ and $B_{\phi,\theta}$ are components of the plasma velocity and magnetic field in poloidal (θ) and toroidal (φ) directions, respectively. However, there is a linear proportionality between T_i and u_Δ in discharges with ITBs in JET [28]. The relationship between Γ and ∇T_i, via the E×B flow, shear is maintained due to $T_i \propto u_\varphi$. Figure 10 shows ion, electron and total heat flux $\Gamma_{i,e,tot}$ crossing the ITB in Pulse No: 58178. The location of the ITB is defined here as the magnetic surface, where $L_{Ti,e} = -T_{i,e}/(dT_{i,e}/dr)$ reaches a minimum. The first point in the graph at t=4.4s corresponds to the time of the ion ITB formation. It should be noted that an electron ITB was formed earlier in the current ramp-up phase with LHCD. The heating power reduction, starting after $t \approx 7s$ (see Figure 1), is accompanied by a reduction by a factor of 2 in Γ_i. Such reduction is reminiscent of the effect of hysteresis. However, the difference between the fluxes at $t = 4.4s$ (ion ITB formation) and $t = 10-13s$ is much smaller. Turbulence stability analysis was performed to

establish the role of different factors such as plasma rotation, ≤-stabilisation and magnetic shear in the ITB sustainment.

The turbulence stability was analysed using the Kinezero code [20]. It is a local linear gyrokinetic code based on a ballooning representation in the electrostatic approximation. The code describes the ITG/TEM and ETG modes, taking into account passing and trapped ions and electrons. The collisions and plasma shaping effects are not included.

The results of Kinezero simulations are shown in Figure 11 for two time slices at t = 9s and 13s corresponding to the beginning and end of the power step down phase in Pulse No: 58178. It should be noted, that condition $T_e \approx T_i$ is a characteristic feature of the electron and ion transport barriers in this discharge and in JET plasmas in general. Qualitatively, the results are very similar for both time slices. The main difference is in the location of the ITB due to the footpoint shift from r/a⌣0.32 at t = 9s to r/a⌣0.23 at t = 13s. Both ITG/TEM (solid line) and ETG mode (dashed line) growth rates reach their maximum roughly at the same location, which is close to the ITB footpoint. The growth rate of ITG/TEM mode γ_{lin} (Figure 8(a),(b), solid line) exceeds the rotation shearing rate $\omega_{E\times B}$ (dashed-dotted line) in the region, where magnetic shear is positive. The drive for the ITG/TEM and ETG modes decreases sharply, when the magnetic shear changes sign from positive to negative. The location of s = 0 approximately coincides with the ITB footpoint. ITG/TEM and ETG modes are stabilised completely when the magnetic shear becomes sufficiently negative. In this region the rotation shear stabilisation plays a complimentary role. A simulation with parameter $\alpha = -q^2Rd(8\pi nT/B^2)/dr = 0$ as performed to separate the effects of stabilisation due to magnetic shear and finite β-stabilisation. The growth rate for the ITG/TEM mode at $\alpha = 0$ (dotted line) is higher than for the finite α ($0.5 \le \alpha \le 2$) inside the ITB region, which shows that finite β-stabilisation plays an essential role for this range of α's. The ITG/TEM mode is mainly driven by passing ions with some smaller contributions from trapped electrons and trapped ions, as can be seen from the charts in Figure 8c,d. The ETG mode at the location of the maximum growth rate is driven by passing and trapped electrons (not shown in the Figure). The E×B flow shear is comparable to γ_{lin} in a relatively narrow region where the magnetic shear changes sign. This region is located in the vicinity of the ITB footstep. Here the E×B shear may be important for the preventing the growth of the turbulence and the consequent erosion of the ITB and displacement of the foot step.

Additional information on the relative role of the magnetic shear and $\omega_{E\times B}$ in turbulence stabilisation can be obtained from the analysis of the sawtooth-like events, or internal reconnections, typical of discharges with current holes [19]. Such events are caused by MHD instability. Modelling shows that double tearing modes may be triggered in the vicinity of rational q surfaces in reversed shear configurations [29]. The mode flattens the off-axis current density profile, causing a decrease in value of q_o and a moderate reduction in the absolute value of the magnetic shear |s| inside the ITB. However, the strong reversed shear configuration survives. A number of different diagnostics show that each sawtooth like event leads to a reduction in temperature, density and toroidal rotation in the plasma core, as well as an outward shift in the location of the maximum of the gradients of

this parameters inside the ITB region [30]. To illustrate this Figure 12 shows variation of the parameter $\rho_e^* \sim \partial T_e/\partial r$ in space and time. An ITB is associated with the region of the highest ρ_e^*. Two sawtooth events occur at $t_{s1} = 7.85$s and $t_{s2} = 8.26$s. An instantaneous reduction in $\partial T_{e,i}/\partial r$ inside the ITB and an outward shift in the location of maximum of ρ_e^* can be seen at each event. Similar radial shifts should be expected in the maximum of the radial electric field, which is governed by equation $E_r = \nabla P_i/(Z_i e n_i) - u_\theta B_\varphi + u_\varphi B_\theta$. The ion poloidal velocity here is assumed to be neoclassical, which is of the order of $Z_i B_\phi \nabla T_i$. If the plasma turbulence is stabilised mainly by the rotation shear one can expect a radial shift in the ITB location during an MHD event and, possibly, deterioration of the ITB due to reduction in $|E_r|$ (∇P_i, u_θ, u_θ). In practice, the ITB quickly recovers, as seen in Figure 12, after each sawtooth-like event and the maximum of ρ_e^* remains at roughly the same location ($R \cong 3.39$m). This behaviour is in agreement with Kinezero modelling, showing that the main stabilising effect is connected to the strong negative magnetic shear and that this is not affected significantly by the reconnection events.

4. CONCLUSIONS

ITB sustainment was observed in JET discharges with strong shear reversal after a significant reduction in the plasma heating power. The electron ITB was produced during the current ramp-up phase by 2.5MW of LH heating and current drive. The ion and density ITBs were formed by combined NBI, ICRF and LH heating in a current flat-top phase. ITBs were sustained after the combined heating power was reduced from 18MW to 7MW. The mechanism for ITB formation and sustainment was analysed using TRANSP, JETTO, and Kinezero codes.

Modelling of the magnetic configuration, essential for the analysis, was verified by comparison of the pitch angle $\partial = B_\theta/B_\varphi$ measured by MSE diagnostic and calculated by TRANSP. It has been shown that the core ITB was formed and sustained in a negative magnetic shear region. A current hole with strong shear reversal, first produced using LHCD, was maintained for some time by the bootstrap current in the plasma core. The region of negative magnetic shear shrinks with time due to the lack of off-axis non-inductive current outside the ITB region, produced mainly by LHCD. It was demonstrated by modelling that the smaller the poloidal magnetic field B_θ inside ITB the higher is the bootstrap current in accordance with the neoclassical theory. The maximum of the bootstrap current is located in the region of the maximum ∇P. A localised bootstrap current produces shear reversal inside ITB. The ITB foot step is close to the point, where magnetic shear changes sign.

The self-consistent simulation of ITB evolution using JETTO predictive model showed that a reduction in the heat and particle transport is consistent with the turbulence suppression due to the effect of the negative magnetic shear. The plasma rotation shear plays a role in the vicinity of $s = 0$ region, where the effect of negative magnetic shear is insufficient. The LHCD modelling showed that LH current is concentrated in the periphery, when density increases during NBI heating and its effect on the q-profile is relatively weak at the power level of 2.5MW. At an LH power level above 5MW the negative magnetic shear can be produced by LHCD locally at $r/a > 0.6$.

ITG/TEM and ETG mode growth rates γ_{lin} were calculated using Kinezero code to determine the effect of magnetic shear and finite β-stabilisation on the turbulence. It was found that turbulence suppression is expected in the region of negative magnetic shear. The effect of finite β-stabilisation was found to be considerable for $0.5 \leq \varphi = -2q^2Rd(P/B_\varphi{}^2)/dr < 2$. The E×B flow shear was compared with γ_{lin}. It is thought to play a complimentary role in the region of large negative s. However, it can be dominant in a narrow region close to the footpoint of an ITB, where magnetic shear is small ($|s| << 1$) and its effect is insufficient to produce complete stabilisation.

The comparative role of strong negative magnetic shear and E×B flow shear in turbulence stabilisation is supported by the evolution of ITB during internal relaxation in discharges with a current hole. By appearance a long sustainment of the ITB after a significant reduction in the heating power is reminiscent of the effect of hysteresis in the first order transition theory connected with the shear of the plasma rotation [6,7]. The heat flux through the ITB region indeed drops considerably with the reduction of the heating power. However, the mechanism of the heat and particle transport reduction is mainly ascribed to the turbulence stabilisation due to effect of the negative magnetic shear.

ACKNOWLEDGEMENTS.

The authors are grateful to X.Garbet and X.Litaudon for fruitful discussions and recommendations. This work was partly funded by the United kingdom Engineering and Physical Sciences Research Council and EURATOM. This work was performed under the European Fusion Development Agreement.

REFERENCES

[1]. Stambaugh R.D. et al Phys Fluids 1990 **B2** 2941
[2]. Synakowski E.J. Plasma Phys Control.Fusion 1998 **40** 581
[3]. Burrell K.H. Phys Plasmas 1997 **4** 1499
[4]. Challis C.D. 2004 'The Use of Internal Transport Barriers in Tokamak Plasmas' proc. 31st EPS Conf. on Controlled Fusion and Plasma Physics (London, 2004)
[5]. Hahm T.S. Burrell KH Phys Plasmas 1995 **2** 1648
[6]. Terry P.W. Reviews of Modern Physics 2000 **72** 109
[7]. Hinton F.L. Phys Fluids 1991 **B3** 696
[8]. Diamond P.H. et al Phys Rev Letters 1997 **78** 1472
[9]. Diamond P.H. et al Phys Rev.Letters 1994 **72** 2565
[10]. Baranov Yu.F. Plasma Phys Controlled Fusion 2004 **46** 1181
[11]. Challis C.D. et al Plasma Phys Controlled Fusion 2002 **44** 1031
[12]. N.C. Hawkes et al Plasma Phys Control Fusion 2002 **44** 1105
[13]. Joffrin E. et al Nucl.Fusion 2003 **43** 1167
[14]. Pamela J. and JET EFDA Contributors Nucl.Fusion 2003 **43** 1540
[15]. Hawkes N.C. Phys Rev Lett **87** art no115001

[16]. Budny R.V et al Nucl.Fusion 1992 **32** 429
[17]. Tala T.J.J. et al Plasma Phys Control Fusion 2002 **44** A495
[18]. Baranov Yu.F. et al Nucl Fusion 1996 **36** 1031
[19]. Hawkes N.C. et al Plasma Phys Control Fusin 2002 **44** 1105
[20]. Bourdele C. et al Nucl. Fusion 2002 **42** 892
[21]. Fujita T. et al Nuclear Fusion 2002 **42** 180
[22]. Proc 30th EPS Conf.on Contr.Fusion and Plasma Phys., St.Petersburg, 2003, ECA V.27A, P 2.89
[23]. Tresset G. et al Nucl Fusion 2002 **42** 520
[24]. Baranov Yu.F. et al Plasma Phys Control Fusion 2004 **46** 1181
[25]. Kelliher D.J. et al 'Comparison of TRANSP-evolved q-profiles with MSE constrained equilibrium fits on JET Submitted for publication in' Plasma Phys. Control Fusion 2004
[26]. Houlberg W.A. et al Phys Plasmas 1997 **4** 3230
[27]. Weiland J. 'Collective Modes in Inhomogeneous Plasma. Kinetic and advanced fluid theory'. Plasma Physics Theory, Bristol, Phyladelfia , IOP Publishing, 2000.
[28]. Maget P. et al Plasma Phys Control Fusion 2003 **45** 1385
[29]. Huysmans G. Workshop on the Physics of the Current Hole, JAERI-NAKA 2-6 Feb 2004
[30]. Litaudon X. et al Plasma Phys Control Fusion 2002 **44** 1057

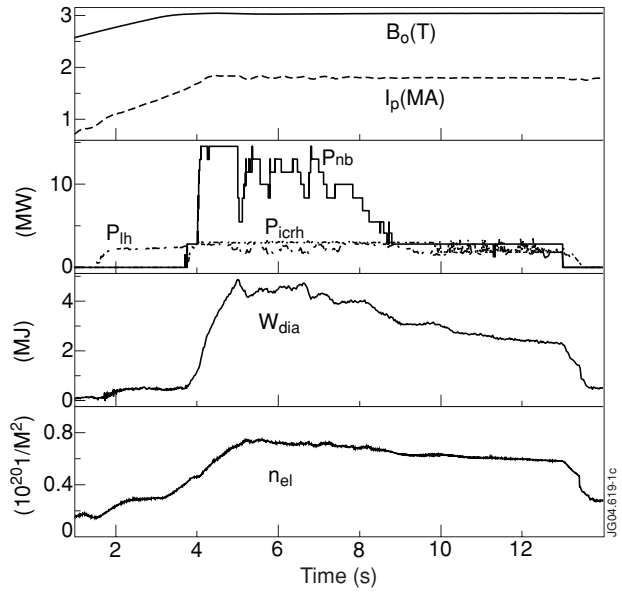

Figure 1: Time traces of magnetic field (B) plasma current (I_p), LH (P_{lh}), NB (P_{nb}) and ICRH (P_{icrh}) power, diamagnetic energy (W_{dia}) and line integrated density (n_{el}). Pulse No: 58178.

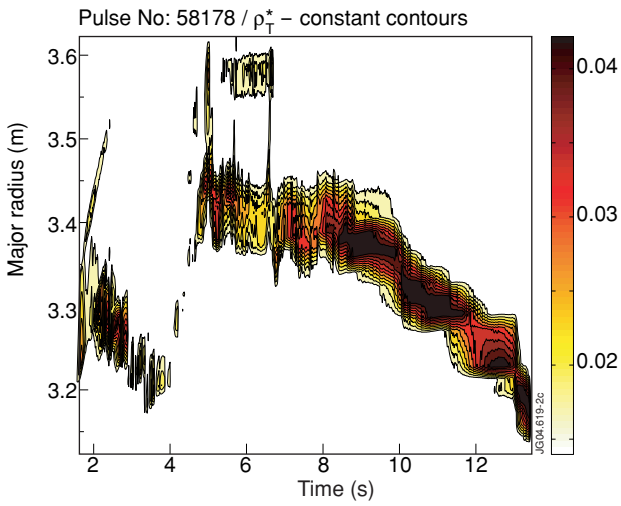

Figure 2: Contour plot of $\rho_e^* = -\sqrt{2m_pT_e/e}\,(dTe/dR) / (B_\varphi Te)$. Pulse No: 58178.

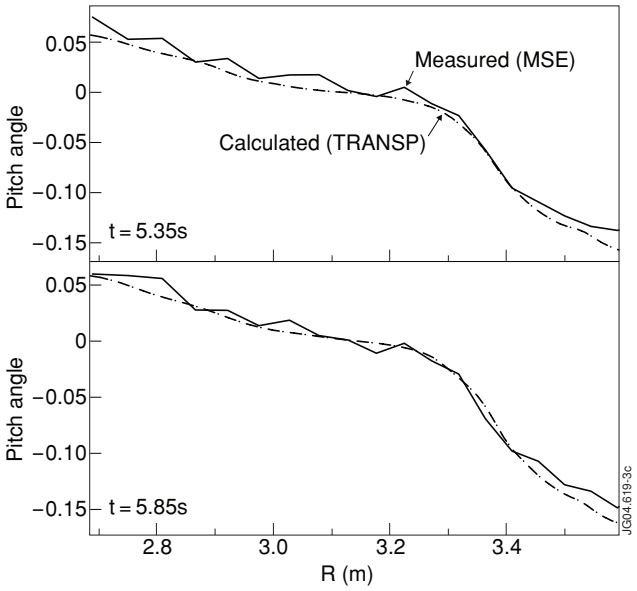

Figure 3: Comparison of calculated using TRANSP code and deduced from MSE measurements pitch angle $\delta = B_p / B_t$. Pulse No: 58178.

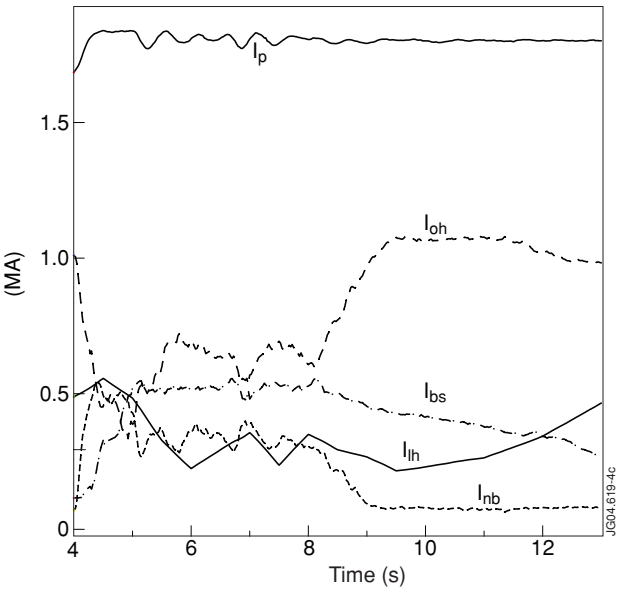

Figure 4: Evolution of the plasma current I_p, Ohmic current I_{oh}, bootstrap current I_{bs}, Neutral beam I_{nb} and LH driven current I_{LH} deduced from TRANSP and LHCD modelling. Pulse No: 58178.

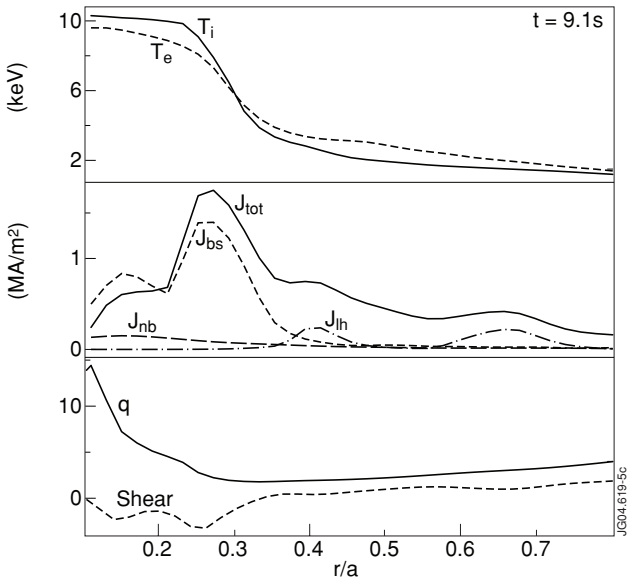

Figure 5: Profiles of T_e, T_i, total current density J_{tot}, bootstrap current J_{bs}, NB driven current J_{nb}, LH driven current J_{lh}, q and magnetic shear at t=9.1s. Pulse No: 58178.

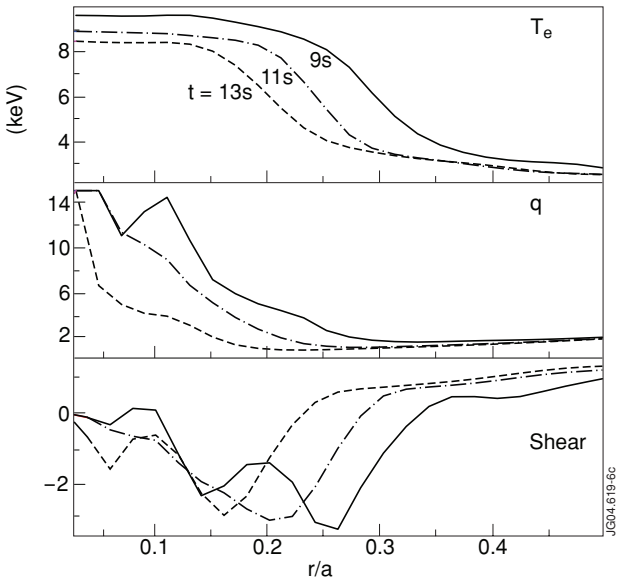

Figure 6: Evolution of T_e, q and shear profiles after power step down. ITB shrinks and follows zero-negative shear region. Pulse No: 58178.

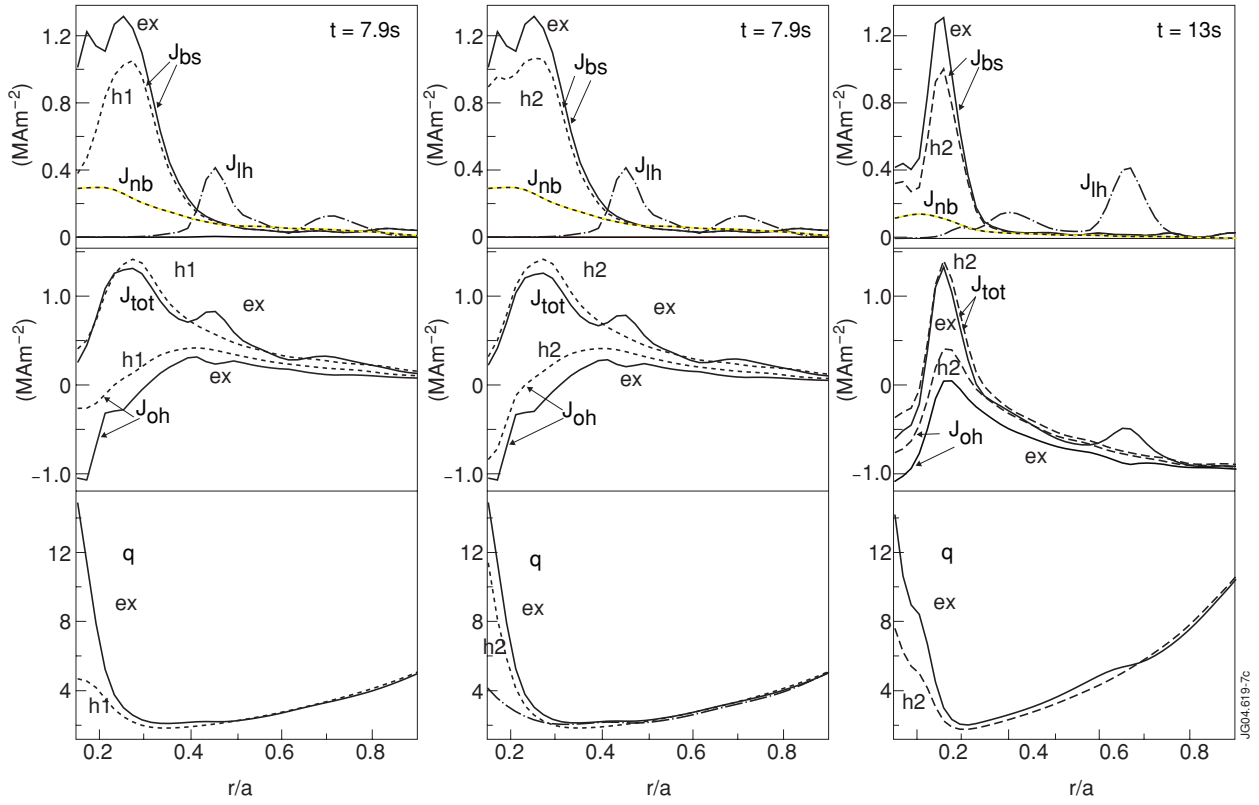

Figure 7: Comparison of current and q profiles for the 'experimental' case 'ex' with hypothetical cases 'h1' and 'h2'. LHCD is applied during preheat and the main heating phase (1.5s ≤ t ≤ 13s) in case 'ex', no LHCD is applied in case 'h1' and LHCD is applied in the preheat phase(1.5s ≤ t ≤ 4s) in case 'h2'. In all cases the measured plasma parameters for Pulse No: 58178 were used in the modelling. (a) cases 'ex' and 'h1' at t= 7.9s, (b) cases 'ex' and 'h2' at t= 7.9s, (c) cases 'ex' and 'h2' at t= 13s. Solid line-case 'ex', dashed line-cases 'h1' and 'h2'. The q-profile shown by thin dashed-dotted line in Fig.7(b) corresponds to modelling as in case 'ex' with j_{bs}=0.

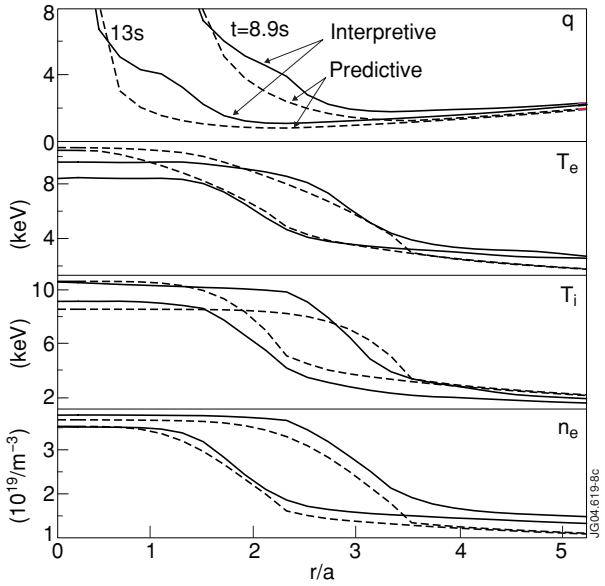

Figure 8. A comparison of the temperature, density and the q-profiles after the heating power step down as deduced from measurements and from the predictive modelling using the JETTO transport model [16]. A parameter $\tau = \alpha_1 + \alpha_2 s + \alpha_3 (\omega_{E\times B}/\gamma_{lin})$ *with* $\alpha_1 = 0$, $\alpha_2 = 1$ *and* $\alpha_3 = 0.1$ *was used in the modelling. The modelling starts at t=6.5s with measured plasma parameters at this time used as initial conditions. The heating and particle sources used in the modelling were deduced from the TRANSP calculations. The calculated bootstrap current was varying from 0.53MA at t=9s to 0.21MA at t=13s, which is close to the result obtained from the TRANSP modelling based on experimental plasma parameters (Figure 4). ITB and current hole shrink and the rate of the ITB footstep movement is close to what observed in the experiment (Figure 6 for comparison).*

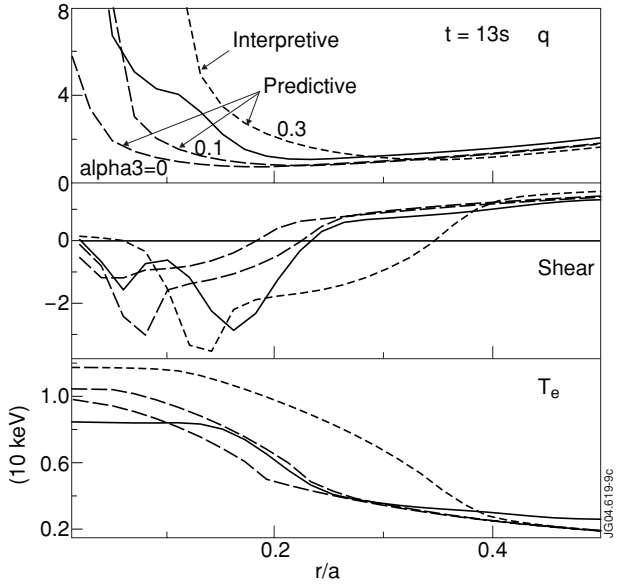

Figure 9: A comparison of the temperature, magnetic shear and the q-profiles at t=13s deduced from the JETTO predictive modelling by varying a parameter α_3 *in the argument* $\tau = \alpha_1 + \alpha_2 s + \alpha_3 (\omega_{E\times B}/\gamma_{lin})$ *of the step function* Θ *at a constant* $\alpha_1 = 0$, $\alpha_2 = 1$. *The initial condition and the plasma heating and particle sources used in the modelling were described in the Figure 8 caption. Results of the interpretative calculations of the q and magnetic shear profiles using experimental temperature and density profiles is shown for comparison. The ITB shrinkage reverses to an expansion as a contribution of the flow shear increases with* α_3. *The best agreement in of the interpretative and predictive calculations is obtained for* $\alpha_2 = 0.1$.

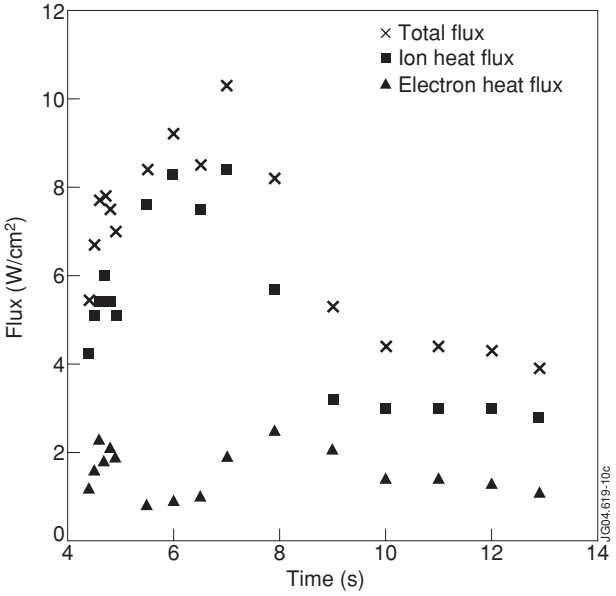

Figure 10: Power flux $\Gamma_{i,e,tot}$ through the ITB as a function of time. First time point at t = 4.4s corresponds to the ion ITB formation time. Electron ITB was formed earlier during LHCD at the current ramp-up phase. Heating power reduction starts at t≈7s, which is accompanied by reduction in $\Gamma_{i,e,tot}$. $\Gamma_{i,tot}$ decrease after t = 10s to the level, which is by factor of 2 smaller than at t = 7s. Such reduction is reminiscent of effect of hysteresis. However, the difference between the fluxex at t = 4.4s and t = 10-13s. is much smaller.

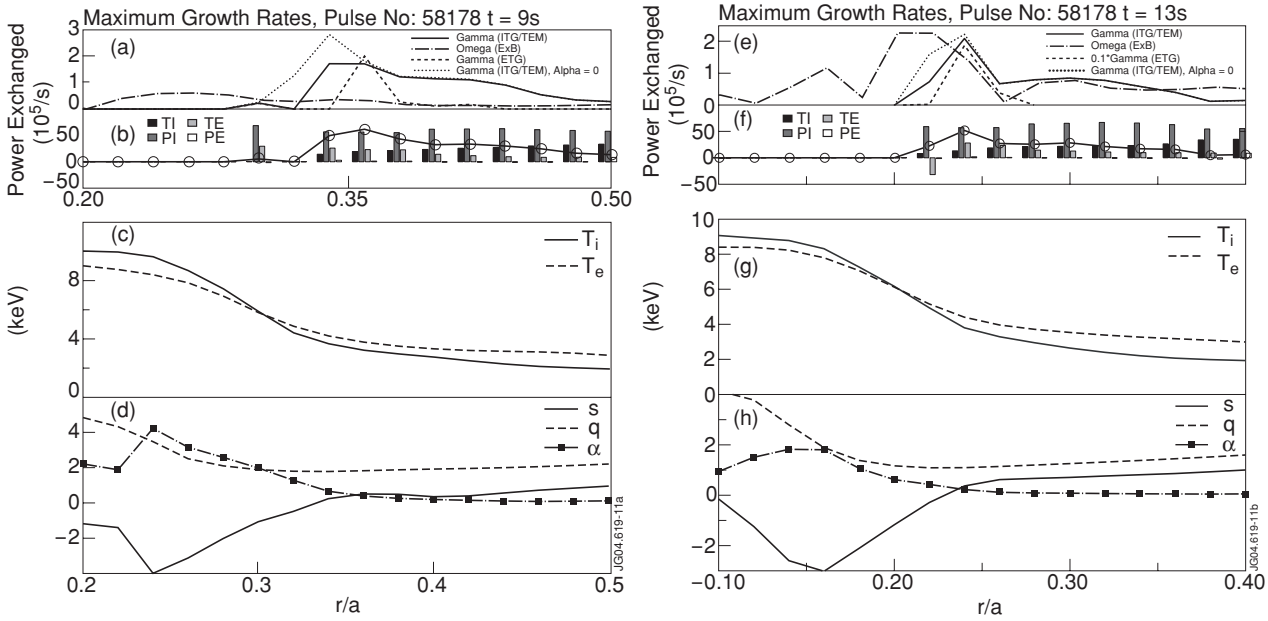

Figure 11: Results of Kinezero modelling: a,e) ITG/TEM, ETG mode growth rate and $\omega_{E\times B}$, b,f) power exchange between ITG/TEM modes and passing electrons-PE, ions-PI and trapped ions TI and trapped electrons TE, c,g) T_e, T_i profiles, d,h) profiles of s, q and $\alpha = -2q^2Rd(P/B^2)/dr$. Pulse No: 58178, a,c,e,g)t = 9s, b,d,f,h) t = 13s.

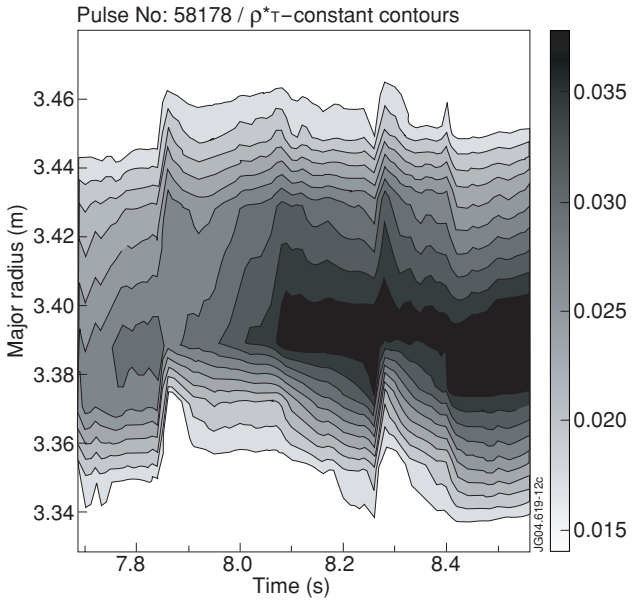

Figure 12. Contour plot of of ρ_e^*. Sawteeth like events occur at t_{s1} =7.85s and t_{s2}=8.26s. ITB associated with max(ρ_e^*) is deteriorated (reduced ρ_e^*) during the sawtooth event and quickly recovers at roughly the same location R ≅ 3.39m. Pulse No: 58178.